THE ASTROPHYSICAL JOURNAL, 484:560–573, 1997 August 1
© 1997. The American Astronomical Society. All rights reserved. Printed in U.S.A.

COSMOLOGICAL MODEL PREDICTIONS FOR WEAK LENSING: LINEAR AND NONLINEAR REGIMES

BHUVNESH JAIN
Max-Planck-Institut für Astrophysik, 85740 Garching, Germany; bjain@mpa-garching.mpg.de
AND
UROŠ SELJAK
Center For Astrophysics, Harvard University, Cambridge, MA 02138; useljak@cfa.harvard.edu
Received 1996 November 13; accepted 1997 March 6

ABSTRACT

Weak lensing by large-scale structure induces correlated ellipticities in the images of distant galaxies. The two-point correlation is determined by the matter power spectrum along the line of sight. We use the fully nonlinear evolution of the power spectrum to compute the predicted ellipticity correlation. We present results for different measures of the second moment for angular scales $\theta \simeq 1'$–3° and for alternative normalizations of the power spectrum, in order to explore the best strategy for constraining the cosmological parameters. Normalizing to observed cluster abundance, the rms amplitude of ellipticity within a 15′ radius is $\simeq 0.01 z_s^{0.6}$, almost independent of the cosmological model, with z_s being the median redshift of background galaxies.

Nonlinear effects in the evolution of the power spectrum significantly enhance the ellipticity for $\theta < 10'$—for $\theta \simeq 1'$ the rms ellipticity is $\simeq 0.05$, which is nearly twice as large as the linear prediction. This enhancement means that the signal-to-noise ratio for the ellipticity is only weakly increasing with angle for $2' < \theta < 2^\circ$, unlike the expectation from linear theory that the signal-to-noise ratio is strongly peaked on degree scales. The scaling with cosmological parameters also changes because of nonlinear effects. By measuring the correlations on small (nonlinear) and large (linear) angular scales, different cosmological parameters can be independently constrained to obtain a model-independent estimate of both power spectrum amplitude and matter density Ω_m. Nonlinear effects also modify the probability distribution of the ellipticity. Using second-order perturbation theory, we find that over most of the range of interest there are significant deviations from a normal distribution.

Subject heading: gravitational lensing

1. INTRODUCTION

Mapping the large-scale structure (LSS) of the universe is one of the major goals of observational cosmology. Traditionally, this is performed using large surveys of galaxies, either the projected two-dimensional distributions or the three-dimensional surveys in redshift space. The main shortcoming of the galaxy surveys is that they trace light, while most of the matter appears to be dark. One therefore needs to translate the galaxy power spectrum into the matter power spectrum, and in order to do so one has to make some assumptions on the nature of galaxy biasing. Even in the simplest model this can be achieved only up to an unknown biasing parameter b, which at present cannot be theoretically estimated. While sophisticated N-body and hydrodynamical simulations will eventually provide some answers to this question, at present the biasing relation between the light and matter remains rather poorly understood and prevents one from drawing definitive conclusions on the amplitude and distribution of mass fluctuations in the universe from galaxy survey data.

It is clearly important to seek ways to estimate the LSS that are insensitive to biasing. Several observable tracers have been proposed that probe directly the underlying mass distribution: cosmic microwave background (CMB) anisotropies, gravitational lensing, peculiar velocity flows, and abundances of massive nonlinear objects. This paper focuses on tracing the dark matter with gravitational lensing, particularly the effects of weak lensing by LSS on background galaxies. Weak lensing magnifies and shears the images of distant galaxies. The shear induces an ellipticity in the image of an intrinsically circular galaxy. Background galaxies are of course not circular, but by averaging over the observed ellipticities of a large number of galaxies, the induced ellipticity can be measured and related to the mass fluctuations along the line of sight and to the spatial geometry of the universe. Ellipticities of distant background galaxies averaged over several arcminute windows are sensitive to the mass power spectrum on scales of 1–10 h^{-1} Mpc. For a given spectrum of mass fluctuations, it is sensitive to the cosmological parameters Ω_m and Ω_Λ. Thus, while strong lensing that leads to multiple images probes nontypical regions of the universe that contain massive halos, weak lensing provides a different and a more direct measure of the mass fluctuations on large scales.

The first calculations of the shear signal due to weak lensing that used modern models for the LSS power spectrum were those of Blandford et al. (1991), Miralda-Escude (1991), and Kaiser (1992), based on the pioneering work by Gunn (1967). Our work generalizes the results of these authors to include the effects of nonlinear evolution of the matter fluctuations for flat as well as open and Λ-dominated cosmologies. Villumsen (1996) has considered some aspects of the linear calculation for open models. Very recently, Bernardeau, van Waerbeke, & Mellier (1996), Kaiser (1997), and Stebbins (1996) have also made the linear calculation for different cosmologies. Our work extends the results of the above authors by using the nonlinear power spectrum, which makes a significant difference on small angular scales of $\theta < 10'$. For the nonlinear calculation we have used the prescription of Hamilton et al. (1991) as implemented by

Jain, Mo, & White (1995) and Peacock & Dodds (1996), who provide accurate power spectra for different models, valid from the linear to the strongly nonlinear regime.

One can take two different approaches in interpreting a possible measurement of the shear signal. The first is to work within the framework of a physical model for the dark matter and background cosmology. Such a model is best normalized to *COBE*, and then its small-scale predictions can be compared to the observational constraints of, e.g., cluster or damped Lyα system abundances, strong lensing statistics or peculiar velocity flows, or, in our case, the shear amplitude on a given angular scale. Another possibility, which is less model dependent, is to compare the constraints from different tracers on the same physical scale. This way, one can test the gravitational instability assumption that both tracers probe the same underlying power spectrum and place constraints on the cosmological parameters, which scale differently with the tracers. At present, the CMB data constrain the power spectrum only on very large scales, where there are no available data from other tracers. While several current CMB experiments are approaching the scales probed by other tracers, cosmological parameters such as baryon density, reionization epoch, and Hubble constant become important and complicate the power spectrum reconstruction. The test mentioned above is possible between the cluster abundances (or strong lensing statistics of multiple images at large separation, both of which trace essentially the same property) and the peculiar velocities. Unfortunately, this method cannot give model-independent constraints on cosmological parameters, because the two tracers scale roughly equally with the matter density Ω_m (Peebles 1980; White, Efstathiou, & Frenk 1993).

A similar comparison can also be made between weak lensing observations and the tracers discussed above. For example, the shear amplitude on 15′ angular scale and rich cluster abundance both probe power spectrum scales around 8 h^{-1} Mpc, so the ratio of the two is roughly independent of the shape of the power spectrum. One could hope that using such comparisons would lead to an estimate of the mean density of the universe, because the two tracers scale differently with it. Unfortunately, as shown in this paper this is not the case, so that this is not a promising method of obtaining the mean density. Nevertheless, weak lensing can also give important constraints on the power spectrum both on smaller and larger scales, where other tracers give less stringent constraints. On the smaller angular scales, our calculations provide the enhancement in the amplitude and the change in the scalings with σ_8 and Ω_m that arise because of nonlinear evolution. Once reliable detections of the shear at different angular scales are available, these results can be used to constrain cosmological parameters and the matter power spectrum. The principal advantage of working with weak lensing is that no assumptions about the formation of observable structures need to be made to connect the mass power spectrum to the observed shear. The only unknown parameter is the redshift distribution of source galaxies, and, in principle, this can also be determined observationally.

In § 2 and the Appendix, the formalism for the weak lensing calculation is presented following Seljak (1995, 1996), who generalized the work by Blandford et al. (1991), Miralda-Escude (1991), and Kaiser (1992) to a nonflat universe and nonlinear regime. The derivation presented here is complementary to recent derivations by Bernardeau et al. (1996) and Kaiser (1997). The linear and nonlinear evolution of the power spectrum is introduced in § 2.1, and the resulting dependence on cosmological parameters for power-law spectra is obtained in § 2.2. In § 3 realistic CDM-like spectra are used to predict the rms shear. We provide accurate power-law fits for the dependence of the shear on the parameters θ, z_s, σ_8, and Ω_m for different cosmological models. Section 3.1 provides predictions of the shear for *COBE* and cluster abundance normalized spectra for the range of angular scales that are being probed by current and forthcoming observations. The effects of non-Gaussianity in the distribution of shear are considered in § 4, where we compute the skewness of the distribution. This is followed by a discussion and conclusions in § 5.

2. THEORY OF WEAK LENSING

Gravitational lensing shears and magnifies the images of distant galaxies. The relation of the shear to perturbations in the gravitational potential along the line of sight is developed in the Appendix. Here we shall use the formalism presented in the Appendix to derive expressions for three different measures of the second moment of the shear.

The observable mean ellipticity of galaxy images can be simply defined in the approximation that the images are ellipses with complex eccentricity ϵ given by the axes lengths b and a as follows: $\epsilon = (b^2 - a^2)/(b^2 + a^2)e^{2i\psi}$, where ψ is the position angle of the major axis. In the limit of weak distortions, the eccentricity is the same as ellipticity $\epsilon \approx (1 - b/a)e^{2i\psi}$. While individual galaxies have intrinsic ellipticities that cannot be separated from gravitational stretching, we have assumed here that averaging over several galaxies leaves only the gravitational component, which can, in principle, be measured. This mean ellipticity $\langle\epsilon\rangle$ will be denoted as $\boldsymbol{p}$ and is defined by equation (A6) in the Appendix. We shall use p to denote its amplitude in what follows.

Information on the ellipticity is contained in the trace-free part of the shear tensor, which is obtained by integrating over all the deflectors between us and the galaxy and over the distribution of background galaxies $W(\chi)$ (see Appendix):

$$\Phi_{ij} \equiv \frac{\partial\,\delta\theta_i}{\partial\theta_j} = -2\int_0^{\chi_0} g(\chi)\nabla_i\nabla_j\phi(\chi)d\chi\ ,$$

$$g(\chi) = r(\chi)\int_\chi^{\chi_0}\frac{r(\chi'-\chi)}{r(\chi')}W(\chi')d\chi'\ . \qquad (1)$$

Here ϕ is the gravitational potential, and χ is the radial comoving distance, with χ_0 being the horizon distance. We also introduced the comoving angular distance $r(\chi)$ defined in equation (A2). The radial distribution of background galaxies is described with the window $W(\chi')$. If all the galaxies are assumed to lie at the same redshift z_s, corresponding to χ_S, then $W(\chi') = \delta_D(\chi' - \chi_S)$, and $g(\chi)$ takes the simple form

$$g(\chi) = r(\chi)\frac{r(\chi_S - \chi)}{r(\chi_S)}\ . \qquad (2)$$

There are several two-point statistics that can quantify the induced ellipticites in galaxy images. The easiest to obtain from observations is the rms ellipticity $\bar{p}(\theta) \equiv \langle\bar{\boldsymbol{p}}(\theta)\bar{\boldsymbol{p}}(\theta)^*\rangle^{1/2}$, where the overbar indicates the average within a circular aperture of radius θ. Equation (1) can be used to express $\bar{p}(\theta)$ in terms of the power spectrum of density perturbations $P_\delta(k, \chi)$. Following the derivation

presented in the Appendix, we obtain for the ellipticity variance

$$\bar{p}^2(\theta) = 9(2\pi)^2\Omega_m^2 H_0^4 \theta^{-2} \int_0^{\chi_0} \left(\frac{g}{ra}\right)^2 d\chi \int P_\delta\left(\frac{l}{r\theta}, \chi\right) W_2^2(l) l\, dl$$
$$= 36\pi^2\Omega_m^2 \int_0^\infty k\, dk \int_0^{\chi_0} a^{-2}(\chi) P_\delta(k, \chi) g^2(\chi) W_2^2[kr(\chi)\theta] d\chi , \quad (3)$$

where $W_2(x) = 2J_1(x)/x$, with $J_1(x)$ being the Bessel function of first order, and a is the expansion factor normalized to unity today. A related quantity is the two-point polarization correlation function $C_{\rm pp}(\theta) = \langle \epsilon(0)\epsilon^*(\theta)\rangle$, which is given by a similar expression to the one above, replacing the term W_2^2 with J_0:

$$C_{\rm pp}(\theta) = 36\pi^2\Omega_m^2 \int_0^\infty k\, dk \times \int_0^{\chi_0} a^{-2}(\chi) P_\delta(k, \chi) g^2(\chi) J_0[kr(\chi)\theta] d\chi . \quad (4)$$

The Fourier transform of $C_{\rm pp}(\theta)$ is the angular ellipticity power spectrum $P(l)$, which is often the optimal statistic to use (Kaiser 1992). Here we use the quantity $\sigma^2(l) = 2\pi l^2 P(l)$, which gives the contribution to the variance per log interval in l and is given by

$$\sigma^2(l) = 36\pi^2\Omega_m^2 l^2 \int_0^{\chi_0} \frac{g^2(\chi)}{r^2(\chi)} a^{-2}(\chi) P_\delta\left[k = \frac{l}{r(\chi)}, \chi\right] d\chi . \quad (5)$$

This gives an estimate of correlations at an angle $\theta = 1/l$.

No assumption on the matter power spectrum has been made in the above expressions, and one can use them both in the linear and nonlinear regime. The nonlinear spectrum is, in general, a nonseparable function of wavenumber and redshift, thus leading to a complicated coupling of the dependences on the distance factors and the growth of perturbations. It also leads to a nonlinear dependence of the predicted ellipticity correlations on the shape and amplitude of the initial power spectrum. Thus, the amplitude of the ellipticity correlations as well as their dependence on cosmological parameters can change in the nonlinear regime (i.e., on small angular scales). In the rest of the paper we shall explore in detail the outcome of these effects of nonlinear evolution.

2.1. *Evolution of the Power Spectrum*

If the gravitational potential changes in time, then its power spectrum will depend on the radial distance χ. In linear theory this dependence is independent of k and can be written in terms of the potential growth factor $F(\chi)$ as $P_\phi(k, \chi) = F^2(\chi) P_\phi(k)$, which gives for the density power spectrum $P_\delta(k, \chi)/a^2(\chi) = F^2(\chi) P_\delta(k) = [(D_+/a)^2](\chi) P_\delta(k)$, where $D_+(\chi)$ is the linear growth factor for the density. This can be approximated as (Lahav et al. 1991)

$$F(\chi) = 2.5\Omega_m a^{-1}(xf + 1.5\Omega_m a^{-1} + \Omega_K)^{-1} ,$$
$$x = 1 + \Omega_m(a^{-1} - 1) + \Omega_\Lambda(a^2 - 1) ; \quad f = \left(\frac{\Omega_m}{ax}\right)^{0.6} . \quad (6)$$

We have ignored the weak Ω_Λ dependence of the logarithmic growth factor. For $a = 1$, this expression simplifies to

$$F(\chi = 0) = 2.5\Omega_m(1 + \Omega_m^{0.6} + 0.5\Omega_m - \Omega_\Lambda)^{-1} . \quad (7)$$

For a flat $\Omega_m = 1$ model the gravitational potential does not change in time in the linear regime and the region in which $g(\chi)$ peaks dominates the radial integral in equations (3), (4), and (5). Typically, this is at half the mean comoving distance to the galaxies, so if background galaxies lie at $z = 1$, then typical deflectors lie at $z \approx 0.3$. In low Ω_m models the gravitational potential increases with χ, differently for open and for cosmological constant models. In the small z limit the growth factor only depends on Ω_m (Villumsen 1996).

On scales where $\Delta^2(k, \chi) = 4\pi k^3 P_\delta(k, \chi)$ approaches or exceeds unity, nonlinear evolution of the power spectrum becomes important. This is particularly important if one is discussing low-Ω_m models, where both cluster abundances and peculiar velocity normalizations give higher density normalization on scales of interest. In the quasilinear regime the nonlinear spectrum can be computed using perturbation theory. An alternative semianalytic approach that is accurate from the linear to the strongly nonlinear regime (up to density contrasts $\sim 10^3$) was proposed by Hamilton et al. (1991) and further developed in subsequent work (e.g., Nityananda & Padmanabhan 1994; Peacock & Dodds 1996; Jain et al. 1995; Padmanabhan et al. 1996). This prescription involves mapping the nonlinear spectrum at a wavenumber k to the linear spectrum at a unique wavenumber $k_L < k$, which is given by a spherical collapse model. This leads to a mapping of the form $\Delta^2(k, \chi) = G[\Delta_L^2(k_L, \chi)]$, where the dimensionless power Δ^2 is defined above, and G is a function that varies in a simple way for different initial spectra. The linear wavenumber k_L is given by $k_L = k[1 + \Delta^2(k, \chi)]^{-1/3}$. The functional form of the mapping is thus specified by the function G, which has been calibrated using high-resolution N-body simulations and is accurate for a wide range of initial spectra.

For the predictions of the rms ellipticity in § 3, we shall use the fitting formulae of Jain et al. (1995) for $\Omega_m = 1$ and of Peacock & Dodds (1996) for the open and Λ models to describe the nonlinear power spectrum as a function of wavenumber and redshift. We refer the reader to the above references for details of the formulae and their implementation. While the formulae can differ by a few tens of percent for certain spectra, we find that our results for the ellipticity are not affected by more than a few percent as the ellipticity integrates the power spectrum over a range of wavenumbers and redshifts. In particular, the results for the CDM-like models shown in Figures 4–9 (see below) would be completely unaffected by our choice of fitting formulae.

2.2. *Dependence on z_s, σ_8, and Ω_m for Power-Law Spectra*

In the next section we shall use the nonlinear evolution of CDM-like spectra to predict the rms ellipticity signal. Here we consider the simplified case of power-law initial spectra $P_\delta(k) = Ak^n$ to compute the scalings of $C_{\rm pp}(\theta)$ and $\bar{p}^2(\theta)$ with source redshift z_s, and the cosmological model parameters σ_8 and Ω_m. The parameter σ_8 is the rms fluctuation in the mass on scales of $8\ h^{-1}$ Mpc, and it serves to normalize the power spectrum. We use the linear evolution of the power spectrum for which some of the scalings can be obtained analytically. We also consider the qualitative modification due to nonlinear evolution by using the stable clustering regime, which gives the maximal effect of nonlinearities. The length scales that contribute to the ellipticity are of order $8\ h^{-1}$ Mpc for $\theta \simeq 15'$. On these scales most realistic spectra have a spectral index $n \simeq -1$. On smaller angular scales, the contribution to the ellipticity comes from higher wave-

numbers, which sample a steeper part of the spectrum (lower n). We therefore choose power-law spectra with $n = -1$ and $n = -2$ for comparison with realistic spectra on angular scales of interest.

For a power-law spectrum the k-integral for $C_{\rm pp}$ is analytic and gives

$$C_{\rm pp}(\theta) = 36\pi^2\Omega_m^2 A \frac{2^{n+1}\Gamma(1+n/2)}{\theta^{2+n}\Gamma(-n/2)} \times \int_0^{\chi_0} d\chi g^2(\chi) r(\chi)^{-2-n} F^2(\chi) , \quad (8)$$

valid for $-2 < n < -\frac{1}{2}$. The constant $A \propto \sigma_8^2$ gives the normalization of the power spectrum. Aside from the numerical prefactors, the result for $\bar{p}^2(\theta)$ is the same and involves the same χ integral.

For simplicity we shall take all the source galaxies to be at the same redshift—this is a good approximation, as the result is insensitive to the source distribution for a given median source redshift. The window function $g(\chi)$ then takes the form given in equation (2). For $\Omega_m = 1$, $r(\chi) = \chi$, and the χ integral is analytic as well, giving the following power-law dependence:

$$C_{\rm pp} , \quad \bar{p}^2 \propto \sigma_8^2 \chi_S^{1-n} \theta^{-2-n} . \quad (9)$$

Using $\chi = 2H_0^{-1}(1 - a^{1/2})$, the dependence of $C_{\rm pp}$ on the source redshift z_s can be obtained from the above equation.

For $\Omega_m < 1$ and $\Omega_\Lambda > 0$, the result for $C_{\rm pp}$ is not analytic except in the limit of $z \ll 1$, which is not of interest for realistic situations. It is simple to understand qualitatively the two physical effects that enter. (1) For a given redshift, the distance χ increases as Ω_m decreases and Ω_Λ increases. Therefore, there is more path length in the line of sight integral, as χ_S is larger for a given z_s. The factor $g(\chi)$ involves factors of the comoving angular diameter distance $r(\chi)$, $r(\chi_S)$, and $r(\chi_S - \chi)$; it also increases with decreasing Ω_m and increasing Ω_Λ. (2) The second factor is the linear growth factor $F(\chi)$. Growth of structure slows down at low redshift in an open universe, and to a lesser extent in a Λ-dominated universe. Therefore, at a given redshift the linear growth factor, normalized to unity today, increases as Ω_m decreases, and for a given Ω_m it decreases as Ω_Λ increases.

The effect of both the distance and growth factors is to increase the contribution from the χ integral in equation (8) relative to the Einstein–de Sitter case. The net contribution increases as Ω_m decreases, and for a given Ω_m, as Ω_Λ increases. In the case of Λ, the distance factors dominate over the linear growth factor, leading to a net increase over the case with the same Ω_m. However, the enhancement due to the integral over χ has to contend with the factor of Ω_m^2 outside the integral, which is considerably larger. The net result is shown in Figure 1 for source galaxies at $z_s = 1$ (*top*) and $z_s = 3$ (*bottom*). The y-axis shows Ω_m^2 times the χ-integrand of equation (8). Thus, $C_{\rm pp}$ or $\bar{p}^2$ is proportional to the area under the curves shown, aside from numerical factors that depend on the shape of the spectrum. The figure shows that the peak contribution for a reasonable choice of z_s comes from the range $z \simeq 0.3$–0.6.

The scaling of $\bar{p}(\theta)$ (the same as that of the square root of $C_{\rm pp}$) with Ω_m is dependent both on z_s and the shape of the power spectrum. For $\Omega_\Lambda = 0$ the dependence is well fitted by the power-law,

$$z_s = 1: \bar{p}(\theta) \propto \sigma_8 \Omega_m^{0.85} . \quad (10)$$

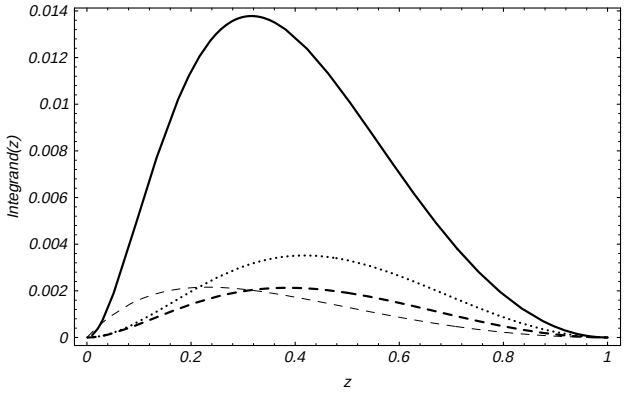

FIG. 1*a*

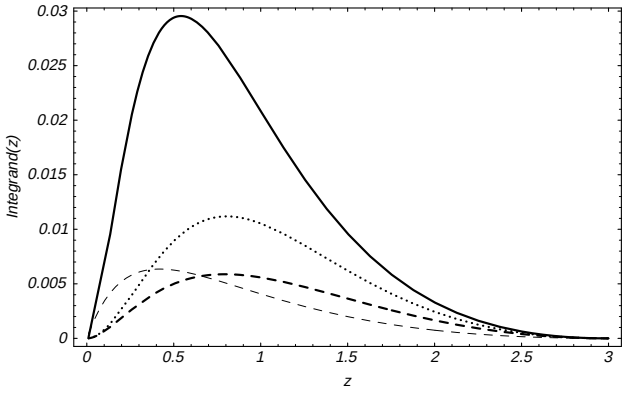

FIG. 1*b*

FIG. 1.—The dependence of the integrand for $C_{\rm pp}$ on redshift. The source galaxies are assumed to be at (*a*) $z_s = 1$ and (*b*) $z_s = 3$, and the matter power spectrum is a power law with slope $n = -2$. The solid line is for $\Omega_m = 1$, the heavy dashed line is for $\Omega_m = 0.3$, $\Omega_\Lambda = 0$, and the dotted line is for $\Omega_m = 0.3$, $\Omega_\Lambda = 0.7$. The figure shows that compared to the Einstein–de Sitter case, the amplitude decreases for the Λ model and is lowest for the open model. The peak of the integrand for $z_s = 1$ lies at about $z = 0.3$ for the $\Omega_m = 1$ case, and it shifts to higher z for the open and Λ models. The thin dashed line is for an $n = -1$ spectrum, with $\Omega_m = 0.3$. It peaks at lower z compared to the heavy dashed line, as the spectrum has more small-scale power.

For $z_s \simeq 1$ and $-2 \lesssim n \lesssim -1$, the above equation is quite accurate. For $z_s = 3$ the scaling depends on the spectrum and can be approximated as follows:

$$z_s = 3: \bar{p}(\theta) \propto \sigma_8 \Omega_m^{0.75} \text{ for } n = -1 ; \quad \bar{p}(\theta) \propto \sigma_8 \Omega_m^{0.6} \text{ for } n = -2 . \quad (11)$$

The result for $n = -2$ is valid, provided a low-k cutoff is imposed to keep the integral finite. As expected, at higher source redshifts the enhancement due to the distance and growth factors is larger and leads to a weaker Ω_m dependence. The same occurs as n decreases, as then there is more power on large scales, and therefore more weight to the high-z part of the integral. The results of equations (10) and (11) are valid for $0.2 \lesssim \Omega_m \lesssim 1$, and are intended to cover the range of source redshift and spectra spanned by realistic models.

A simple way to understand the dependence on Ω_m follows from the fact that most of the lensing contribution comes from about half the distance to the source galaxies. Thus, the Ω_m dependence of equations (10) and (11) can be compared to that of Ω_m at the redshift $z_{1/2}$, corresponding to $\chi_S/2$. $\Omega_m(z_{1/2})$ is well approximated by $\Omega_m^{0.8}$ for $z_s = 1$ and by $\Omega_m^{0.6}$ for $z_s = 3$ if $n = -2$. For a shallower slope there is

more power on small scales, which are closer for a given angle. Hence, the results are closer to those of equations (10) and (11) for $n = -1$ if one uses $\chi_S/3$ [it makes very little difference if one uses $r(\chi)$ instead of χ for this purpose]. Thus, as a first approximation the Ω_m dependence can be obtained by replacing the Ω_m term in $C_{\rm pp}$ for the flat case, by the value of Ω_m at one-third to one-half the distance to the source galaxies.

The above scalings are derived using linear evolution of the power spectrum. On smaller angular scales, nonlinear evolution could play an important role—in the next section we compute the change in the above scalings due to nonlinear effects. It is complicated to estimate the angular scale where nonlinear effects are important because each angle involves the projection of a range of length scales at different redshifts. The answer will therefore depend on the slope of the power spectrum. A rough estimate of the length scales that make the dominant contribution to $\bar{p}(\theta)$ is given by Figure 2. This figure shows the transverse distance for a given θ at the redshifts estimated from Figures 1*a* and 1*b* as providing the dominant contribution to $\bar{p}$ for source galaxies at $z_s \sim 1$–2. For $\theta < 10'$ this length scale is less than 5 h^{-1} Mpc, which is the correlation length of galaxies and therefore a good demarcation of the nonlinear regime. We may thus expect that the linear results for $\bar{p}$ will be modified for $\theta < 10'$.

An analytic estimate of the change in the above scalings due to strongly nonlinear effects can be made using the stable clustering solution. If one assumes that the lensing is dominated by clustering on small scales (valid in the limit of small angles and low source redshift), which stabilized at high redshift, then the dimensionless power is a function of the physical wavenumber times a^3. This property extends to the open models as well, because at high enough redshift, $\Omega_m(z) \simeq 1$. It can then be shown that, if the linear spectrum is normalized to the same σ_8 today, then the enhancement factor of the nonlinear spectrum relative to the linear one is proportional to $F(\chi)^{-3}$. This follows from a reversed version of the argument of Peacock & Dodds (1996), which was made for spectra normalized to the same initial value. A particularly simple example is provided by the $n = -2$ spectrum, for which the nonlinear slope and growth in the Einstein–de Sitter case are the same as in the linear regime.

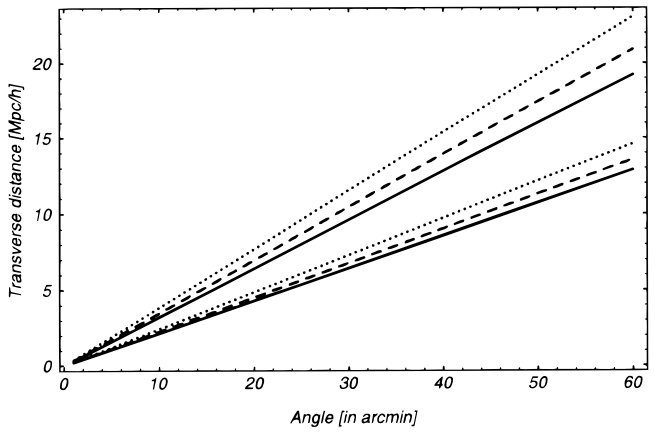

FIG. 2.—The transverse distance at $z = 0.3$ (*bottom set of lines*) and $z = 0.5$ (*top lines*) is shown as a function of the angle. The three curves at each redshift are as in Fig. 1. The two redshifts are chosen to span the range of redshifts that provide the peak contribution for source galaxies at $z_s \sim 1$–2.

Hence, the nonlinear spectrum is given at all k by a constant enhancement factor relative to the linear spectrum.

For $0.3 \lesssim \Omega_m \lesssim 1$ one can approximate $F(\chi) \simeq \Omega_m^{0.5}$ for $z_s \simeq 1$. Therefore, the Ω_m dependence in $\bar{p}^2(\theta)$ due to strongly nonlinear evolution of the power spectrum is $F(\chi)^{-3} \sim \Omega_m^{-1.5}$. In this regime then, $\bar{p}^2 \propto \Omega_m^{0.5}$ times the contribution of the distance factors, which further lowers the power of Ω_m. This estimate is meant to provide an upper bound on the enhancement for open models due to the nonlinear contribution. For realistic redshifts the contribution from such small scales does not dominate, and the exact, numerical estimates of the nonlinear spectrum must be integrated over k and χ. Still, it is clear that the Ω_m dependence of weak lensing amplitude will be significantly weaker than the linear relation predicted from the scalings in the previous subsection.

3. PREDICTIONS FOR RMS ELLIPTICITY FOR COLD DARK MATTER–LIKE SPECTRA

The detailed predictions for the rms ellipticity depend on the shape and amplitude of the power spectrum, the distribution of source galaxies, and on the cosmological parameters Ω_m and Ω_Λ. In the following subsection we shall consider two alternative normalizations of realistic cold dark matter (CDM)–like power spectra. A useful, model-independent description of the scalings can also be obtained by fitting the dependence on the different parameters to power laws. This provides a reasonably accurate approximation to the result and shows the qualitative behavior more clearly.

Table 1 provides such power-law fits to the scalings of $\bar{p}$ with θ, z_s, σ_8, and Ω_m for Einstein–de Sitter, open, and Λ-dominated cosmologies. The three specific models we have chosen are: Einstein–de Sitter ($\Omega_m = 1$, $\Omega_\Lambda = 0$), open ($\Omega_m = 0.3$, $\Omega_\Lambda = 0$), and Λ-dominated ($\Omega_m = 0.3$, $\Omega_\Lambda = 0.7$). The latter two models are representative of the class of open and flat Λ-dominated cosmologies, as the results do not change significantly for Ω_m in the range $0.2 < \Omega_m < 0.5$. The matter power spectrum used in the calculations is the non-

TABLE 1

SCALING OF POLARIZATION $\bar{p}(\theta)$ WITH θ, z_s, AND COSMOLOGICAL MODEL PARAMETERS

θ	z_s	σ_8	Ω_m	Ω_Λ
$\theta^{-0.37}$	1	1	1	0
$\theta^{-0.47}$	1	1	0.3	0
$\theta^{-0.42}$	1	1	0.3	0.7
2′–5′	$z_s^{0.6-0.57}$	1	1	0
15′	$z_s^{0.56}$	1	1	0
2′–5′	$z_s^{0.66-65}$	1	0.3	0
15′	$z_s^{0.67}$	1	0.3	0
2′–5′	$z_s^{0.77-74}$	1	0.3	0.7
15′	$z_s^{0.74}$	1	0.3	0.7
2′–5′	1	$\sigma_8^{1.25-1.20}$	1	0
2′–5′	1	$\sigma_8^{1.38-1.34}$	0.3	0
2′–5′	1	$\sigma_8^{1.29-1.27}$	0.3	0.7
2′–5′	1	1	$\Omega_m^{0.66-0.75}$	0
15′	1	1	$\Omega_m^{0.81}$	0
2′–5′	1	1	$\Omega_m^{0.60-0.65}$	0.7
15′	1	1	$\Omega_m^{0.68}$	0.7
2′–5′	3	1	$\Omega_m^{0.60-0.65}$	0
15′	3	1	$\Omega_m^{0.80}$	0

linear $\Gamma = 0.25$ CDM spectrum, where Γ is the shape parameter defined in Bardeen et al. (1986) and roughly corresponds to $\Omega_m h$ in CDM models. The scalings given in Table 1 are not strongly sensitive to the shape of the power spectrum as shown in Figure 7 (see below) and discussed in the next subsection.

On scales $\theta < 10'$ nonlinear evolution makes a significant difference to all the scalings. Figure 3 shows the ratio of $\bar{p}(\theta)$ computed using the nonlinear/linear power spectrum for the above three models. The ratio is significantly larger than unity for $\theta < 10'$ and reaches a factor of 2 for $\theta \sim 1'$. It is the largest for the open model, where the nonlinear effects are more important because of a slower linear growth of perturbations.

Since the scalings differ in the linear and nonlinear regimes, Table 1 gives power-law fits for three different angles, $\theta = 2'$, $5'$, $15'$, to represent the nonlinear, weakly nonlinear, and linear regimes, respectively. These give $\bar{p}(\theta)$ to good accuracy over most of the range: $1' < \theta < 30'$; $0.5 < z_s < 3$; $0.5 < \sigma_8 < 2$; $0.2 < \Omega_m < 1$. The results can be approximated by the following equations for the three cosmological models given above. The angle θ below is in arcminutes, and where the scalings differ on $2'$ and $15'$, the latter scaling is given in parentheses. Since the scaling with z_s is nearly the same for the two values of θ, we have used an intermediate value in the following equations:

$$\begin{aligned}
\bar{p}[2'(15')] &= 0.08\theta^{-0.37} z_s^{0.58} \sigma_8^{1.25(1)} \\
&\quad \times \Omega_m^{0.66(0.81)}: \Omega_m = 1.0 \\
\bar{p}[2'(15')] &= 0.04\theta^{-0.47} z_s^{0.66} \sigma_8^{1.38(1)} \\
&\quad \times (\Omega_m/0.3)^{0.66(0.81)}: \Omega_m = 0.3 \\
\bar{p}[2'(15')] &= 0.04\theta^{-0.42} z_s^{0.76} \sigma_8^{1.29(1)} \\
&\quad \times (\Omega_m/0.3)^{0.60(0.68)}: \Omega_\Lambda = 0.7 \, . \qquad (12)
\end{aligned}$$

These power-law fits can be used to obtain predictions for the rms ellipticity for any desired choice of cosmological parameters. For $\theta = 15'$, the results are consistent with the linear theory estimates for power-law spectra (with n between -1 and -2) obtained in the previous section. The $\bar{p}(\theta)$ curve is enhanced at small angles because of nonlinear evolution. This enhancement causes the dependence on θ to be much closer to a power law over the range $1' < \theta < 30'$ than the linear prediction, which has much greater curvature because of the curvature of the power spectrum. This power law is steeper for the open and Λ models because of stronger nonlinear evolution.

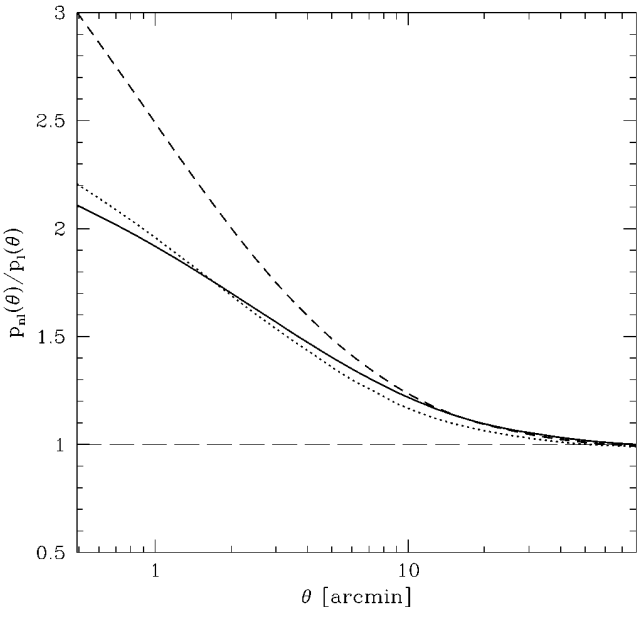

FIG. 3.—The ratio of $\bar{p}(\theta)$ computed using the nonlinear spectrum to that with the linear $\Gamma = 0.25$ CDM spectrum is shown. The normalization is $\sigma_8 = 1$, and $z_s = 1$. The solid line is for $\Omega_m = 1$, the dashed line is for $\Omega_m = 0.3$, and the dotted line is for $\Omega_m = 0.3$, $\Omega_\Lambda = 0.7$. The results show the significant enhancement in $\bar{p}(\theta)$ due to nonlinear evolution for $\theta < 10'$.

On $\theta \simeq 2'$, the dependence on σ_8 is significantly stronger than linear, especially for the open model. Nonlinear evolution also weakens the dependence on Ω_m, as anticipated in the previous section. Combining the scaling with σ_8 and Ω_m (relevant for comparison with other tracers), $\bar{p}(\theta)$ for $\theta \simeq 2'$ scales as $\sigma_8^{1.25}\Omega_m^{0.66}$, whereas on large scales of $\theta > 10'$, it scales as $\sigma_8 \Omega_m^{0.8}$. Thus, on small scales $\bar{p}(\theta)$ measures $\sigma_8 \Omega_m^{0.5}$ (the power of Ω_m is even lower for $\theta < 2'$ or $\Omega_m < 0.5$), whereas on large scales it measures $\sigma_8 \Omega_m^{0.8}$.

Using the above differences, a comparison of $\bar{p}(\theta)$ at small and large angular scales can constrain σ_8 and Ω_m separately. Thus, nonlinear evolution, at the expense of a more complex dependence on various parameters, can help break the degeneracy between these parameters. To distinguish an open from a flat Λ-model with the same value of Ω_m, one needs to use the difference in the scaling with z_s, as the other scalings are very similar. The Λ-model predicts a faster increase with z_s because of a faster increase of the distance factors with redshift than the open case. Once it becomes feasible to get estimates of the redshifts of source galaxies, this difference can become a useful test of Λ, as it is nearly independent of the shape and normalization of the power spectrum.

3.1. *Results for Cluster Abundance and COBE Normalized Spectra*

In choosing the most realistic power spectrum to compute the polarization signal, the approach closest to other tracers of the mass density field would be to use the abundance of galaxy clusters or the peculiar velocity field of galaxies to estimate the amplitude σ_8, and to then use the galaxy power spectrum to constrain the shape (Peacock & Dodds 1996; Peacock 1996). The merit of this approach is that it agrees with the observational constraints on the scales that are most relevant for weak lensing observations. An alternative is to work with physical models for the dark matter and cosmology that give the shape of the power spectrum and use *COBE* normalization to fix the spectrum on very large scales and thus its overall amplitude. The merit of this approach is that for a given model both the spectrum of perturbations and their evolution is fully determined. However, the final spectrum may or may not agree with the present-day observations (which interpretation is still somewhat uncertain). We shall present results using both approaches.

The first of the two reliable tracers of mass fluctuations on large scales is the abundance of large galaxy clusters with a typical mass of $10^{15}\ M_\odot$, which corresponds to a linear scale of about $8\ h^{-1}$ Mpc. These objects are very rare and according to the Press-Schechter formalism (Press & Schechter 1974), their number density depends exponentially on the amplitude of mass fluctuation on the corresponding linear scale. This allows an accurate estimate of the amplitude, which typically gives $\sigma_8 = 0.5$–0.6 (White,

Efstathiou, & Frenk 1993; Viana & Liddle 1996; Eke, Cole, & Frenk 1996; Pen 1997) in an $\Omega_m = 1$ universe, almost independent of the shape of the power spectrum. At present this gives the best constraint on the linear density power spectrum, with an error of about 10%–20%. The dependence on Ω_m is approximately $\sigma_8 \propto \Omega_m^{-(0.5-0.6)}$ and differs only slightly for open and spatially flat models. The scaling with Ω_m and Ω_Λ is still somewhat uncertain, as it requires calibration with large N-body simulations.

Peculiar velocities are also tracers of underlying mass fluctuations. In the linear regime there is a simple relation between velocity and density fields (Peebles 1980): $\delta(r) = -(H_0 f)^{-1} \nabla \cdot v(r)$, where $f \simeq \Omega_m^{0.6}$. The Ω_m dependence on mass fluctuation amplitude from velocity data is $\sigma_8 \propto \Omega_m^{-0.6}$, which is almost the same as for the cluster abundance in a flat universe and only slightly less so in an open universe. Comparison of the two constraints therefore cannot significantly constrain Ω_m. Given a set of velocity measurements, one can reconstruct the particular combination $f\delta$ and estimate its power spectrum. Recent comparisons between Mark III Tully-Fisher catalogs and the *IRAS* survey tend to favor $\beta_I = \Omega^{0.6}/b_I \sim 0.5$ (Willick et al. 1997; Davis, Nusser, & Willick 1996), where b_I is the linear bias parameter for *IRAS* galaxies. This combined with $\sigma_{8,I} \sim 0.7$ leads to $\sigma_8 \Omega^{0.6} = 0.35$, smaller than the value derived from the cluster abundance data. This would therefore reduce the weak lensing predictions presented in this paper. However, analysis of Mark III catalog with POTENT gives a higher value of $\sigma_8 \Omega^{0.6}$ (Kolatt & Dekel 1997), so it seems prudent to adopt the cluster abundance normalization until the discrepancy in the velocity data is resolved.

Based on the above discussion, a useful functional form for the density power spectrum is given by a CDM-type transfer function with two free parameters, the amplitude $\sigma_8 \approx 0.6\Omega_m^{-0.6}$ and the shape parameter $\Gamma \approx 0.25$ (Peacock & Dodds 1996). This is the model that will be adopted in computing predictions of ellipticity polarizations for cluster abundance normalization. We shall use the fitting formulae in equations (47)–(49) of Viana & Liddle (1996) to compute σ_8 as a function of Ω_m—their normalization is very close to the results of White, Efstathiou, & Frenk (1993) and Pen (1997), though a bit higher than that of Eke et al. (1996).

Before proceeding with the results for $\bar{p}(\theta)$, we consider the contribution to the integral from different ranges in k. Figure 4 compares the contribution per logarithmic interval in wavenumber to $\bar{p}^2$ and $\sigma^2(l)$ at $\theta = 15'$, $z_s = 1$ with the logarithmic contribution to σ_8^2, which is also an integral of the power spectrum over k with a real space top-hat filter. All the distributions are normalized so that they peak at unity. One can see that the distribution of $\bar{p}^2$ is broader and that of $\sigma^2(l)$ narrower than the corresponding σ_8^2 distribution, but, in general, they sample very much the same scales. Thus, the optimal statistic to use in order to compare the normalization σ_8 with other tracers is $\sigma^2(l)$, $\bar{p}^2(\theta)$ at $1/l$, $\theta \simeq 15'$. The comparison can then be made nearly independent of the shape of the power spectrum.

We need to choose a redshift distribution for the source galaxies in order to compute $\bar{p}(\theta)$. At present this is spectroscopically known only for galaxies with magnitude in I below 23 (Lilly et al. 1996; Cowie et al. 1996), which have median redshift $z \sim 0.5$, while typical lensing observations reach several magnitudes deeper (e.g., Mould et al. 1994). *Hubble Space Telescope* observations of Abell 2218 coupled with cluster mass reconstruction indicate that the median redshift increases from $z \sim 0.5$ at $R = 22$ to $z \sim 1$ at $R = 25$ (Kneib et al. 1996). There could, however, be a population even at redshift beyond 1, as indicated by the detection of the shear around a $z = 0.8$ cluster (Luppino & Kaiser 1997). Most of the results we present are for $z_s = 1$, but they can be adapted to any desired z_s using the scalings of Table 1. For simplicity, we have assumed that all the galaxies are at the same distance. This is the best possible case in the sense that it makes the distributions in k space more narrow than for more realistic cases. Fortunately, the difference between our results and those using a different, more realistic distribution of source galaxies with the same median redshift is usually very small (Kaiser 1992; Villumsen 1996).

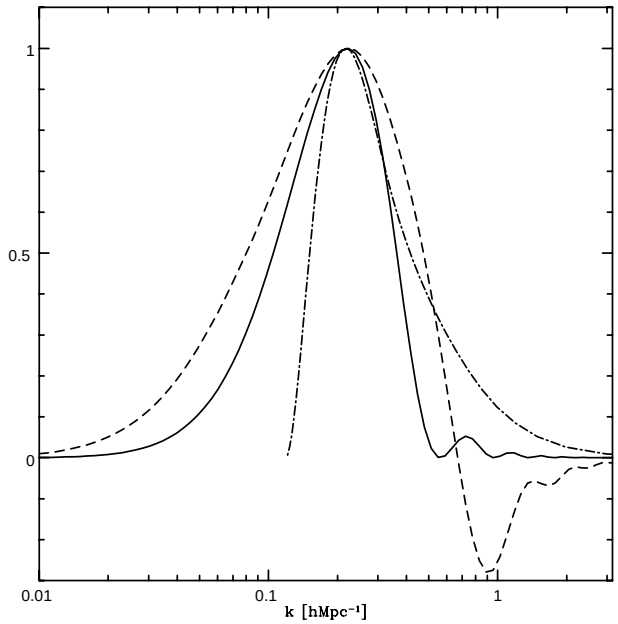

FIG. 4.—The logarithmic contribution from wavenumbers k to C_{pp} (*dashed line*) and $\sigma^2(1/\theta)$ (*dot-dashed line*) at $\theta = 15'$, $z = 1$ is shown. It is compared to that of σ_8^2 (*solid line*), the variance in density on the $8h^{-1}$ Mpc scale. The dependence of $\bar{p}^2$ is nearly the same as that of C_{pp} up to $k \simeq 0.5\ h$ Mpc^{-1}, after which it remains positive, while C_{pp} goes negative.

Figure 5 shows the dependence of $\bar{p}(\theta)$ on θ for the three cosmological models, all with shape parameter $\Gamma = 0.25$, except for the $\Omega_m = 1$ *COBE*-normalized model. The thick solid line is for $\Omega_m = 1$, the dashed line is for $\Omega_m = 0.3$, and the dotted line is for $\Omega_m = 0.3$, $\Omega_\Lambda = 0.7$. The normalization chosen is (*a*) $\sigma_8 = 1$, (*b*) cluster abundance, and (*c*) *COBE*. For the open and flat *COBE* models, we have used $\Omega_m = 0.4$ so that the value of h and σ_8 are reasonable. The three *COBE* models are the following: flat, $\Omega_m = 1$, tilted with $n = 0.8$, $h = 0.5$, $\sigma_8 = 0.72$; open with $\Omega_m = 0.4$, $h = 0.65$, $\sigma_8 = 0.64$; flat, Λ-model with $\Omega_m = 0.4$, $h = 0.65$, $\sigma_8 = 1.07$ (Bunn & White 1997). Since the Λ-model chosen has a high σ_8, it turns out to have nearly the same $\bar{p}(\theta)$ prediction as the tilted $\Omega_m = 1$ model.

The thin solid line is computed using the linear spectrum for the $\Omega_m = 1$ model. As expected from the results of Figure 3, it is only for $\theta > 10'$ that the linear and nonlinear curves start to coincide. For cluster abundance normalization, the amplitude of ellipticity correlations very weakly depends on the mean density for a reasonable range of Ω_m. The enhancement for low Ω_m models from the growth and distance factors discussed in § 2 nearly cancels out the $\Omega_m^{0.4}$ dependence one might have expected from the term outside

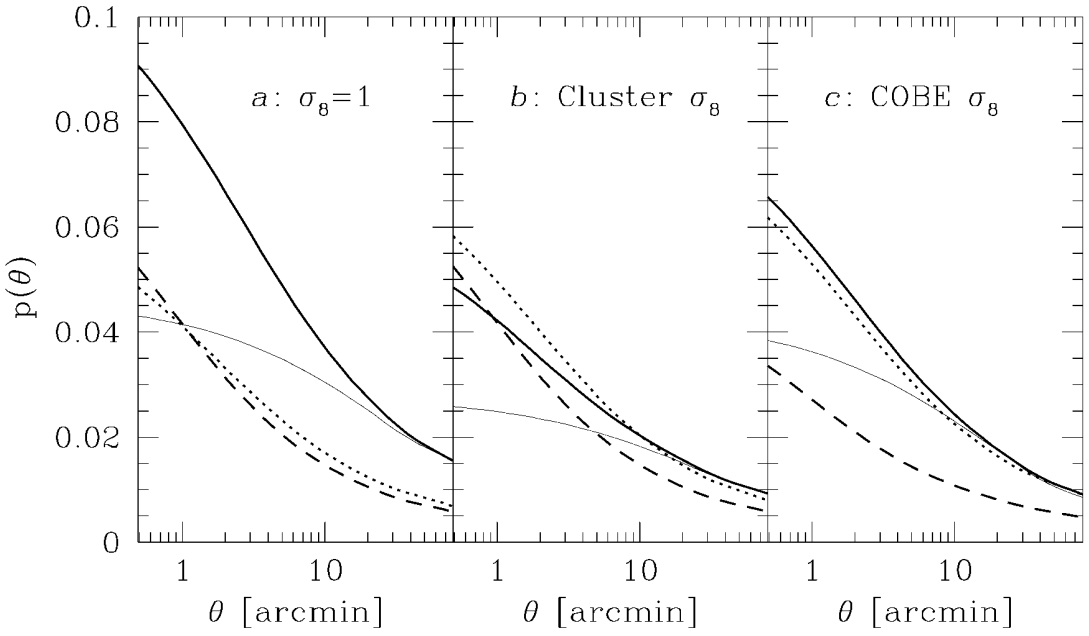

FIG. 5.—The dependence of $\bar{p}$ on θ is shown for three cosmological models, with $z_s = 1$ and a $\Gamma = 0.25$ CDM spectrum. The heavy solid line is for $\Omega_m = 1$, the dashed line is for $\Omega_m = 0.3$, and the dotted line is for $\Omega_m = 0.3$, $\Omega_\Lambda = 0.7$. The thin solid line is for the linear spectrum with $\Omega_m = 1$. The three panels show three alternative normalizations of the power spectrum. In the case of *COBE* normalization, $\Omega_m = 0.4$ has been used for the open and Λ models (see text for details of the other parameters for the *COBE* models).

the integral in equation (3). Therefore, one has to make subtler comparisons of the signal at small and large θ to break the degeneracy between σ_8 and Ω_m. This was discussed above following equation (12). It indicates that comparing weak lensing measurements over different scales can more powerfully constrain Ω_m than comparing the weak lensing amplitude with other tracers. For *COBE* normalization on the other hand, a detection of the correlated ellipticity with reasonable error bars can immediately constrain the cosmological model in question, but of course there might still remain several different models that equally well fit the data.

The effect of choice of statistic, shape of the power spectrum, and the redshift of source galaxies is shown in Figures 6 and 7. Figure 6 shows $\sigma(1/\theta)$ for the three cosmological models with cluster abundance and *COBE* normalization, as in Figure 5. The curves for σ flatten at small θ more than the $\bar{p}$ curves. This is to be expected because $\bar{p}$ integrates over all scales larger than $r\theta$ (where r is the typical distance) and so can only increase toward small scales. Because there is little power on very small scales, it eventually saturates (this typically happens on subarcminute scales; see Keeton, Kochanek, & Seljak 1997). The Fourier space quantity $\sigma^2(l)$, on the other hand, receives contributions only from scales

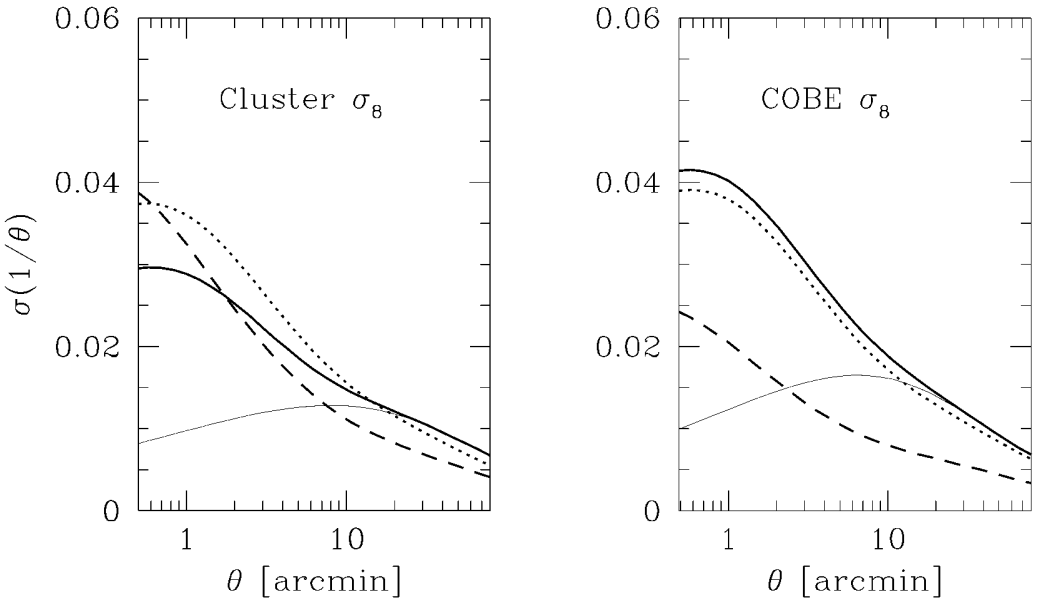

FIG. 6.—The square root of the dimensionless ellipticity power spectrum $\sigma(1/\theta)$ is shown for the same three cosmological models as in Fig. 5. The left panel uses cluster abundance normalized spectra, while the right panel uses *COBE* normalized spectra. The thin solid line shows $\sigma(1/\theta)$ for the $\Omega_m = 1$ model computed using the linear power spectrum.

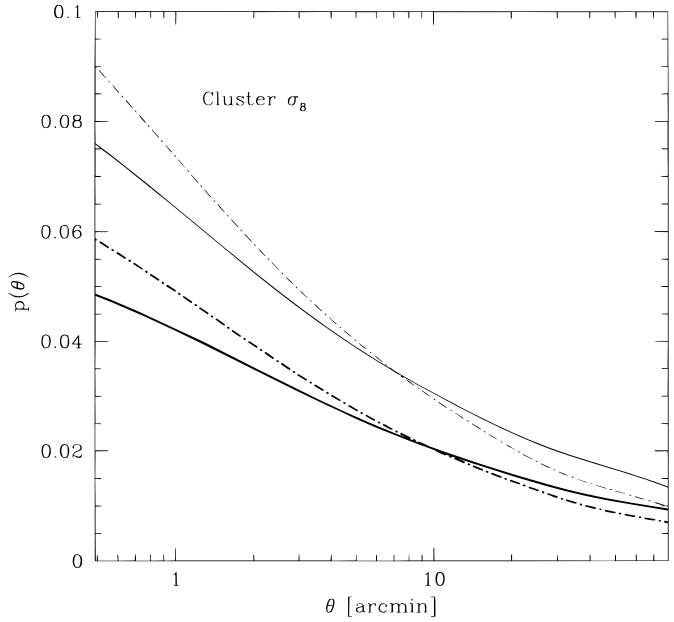

FIG. 7.—The effect of the shape of the power spectrum on $\bar{p}(\theta)$ is shown by comparing the $\Gamma = 0.25$ CDM spectrum (*solid lines*) with the $\Gamma = 0.5$ CDM spectrum (*dot-dashed lines*). The top set of curves is for $z_s = 2$, and the bottom set is for $z_s = 1$. The $\Gamma = 0.5$ spectrum has more small-scale power and therefore predicts larger $\bar{p}$ values at small θ.

smaller than r/l and therefore decreases on very small scales for realistic power spectra. The shape of the C_{pp} curve is very similar to that of $\bar{p}^2$, and for $\theta \gtrsim 2'$, C_{pp} is well approximated by $0.7\bar{p}^2$. Figure 7 compares $\bar{p}(\theta)$ for the $\Gamma = 0.5$ CDM spectrum to the $\Gamma = 0.25$ spectrum used in the rest of the figures. The top and bottom set of curves are for $z_s = 2$ and 1, respectively. Since the $\Gamma = 0.5$ spectrum has more power at small scales, it leads to a larger $\bar{p}$ at small θ. The curves cross around $\theta = 10'$, but the difference is not large for $\theta > 2'$. Figure 8 shows the variation of $\bar{p}(\theta)$ with z_s for $\theta = 15'$ and $\theta = 2'$. The models shown are the same as in the cluster abundance normalized panel of Figure 5. As shown in Table 1, p increases with z_s fastest for the Λ-models.

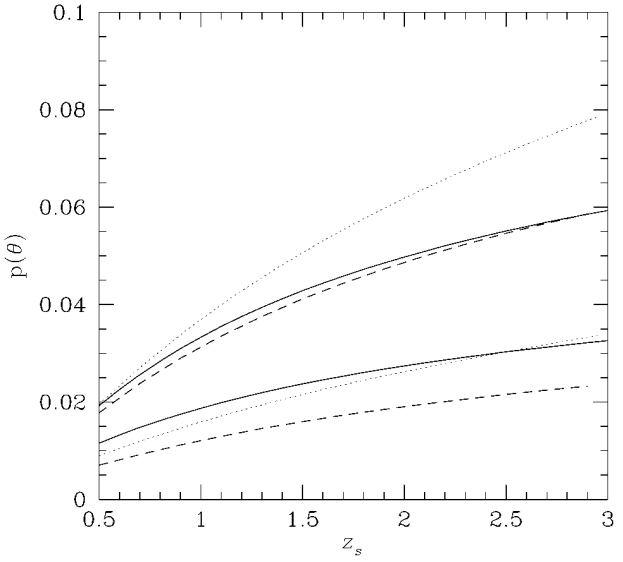

FIG. 8.—The effect of increasing source redshift z_s on $\bar{p}(\theta)$ is shown for $\theta = 2'$ (*top three lines*) and $\theta = 15'$ (*bottom lines*). The three models shown are the same as in Fig. 5 and use cluster abundance normalized spectra. The Λ models, shown by the dotted lines, predict the fastest growth with z_s, as discussed in the text.

4. NONLINEAR EFFECTS ON THE DISTRIBUTION OF ELLIPTICITY

So far we have only discussed the importance of nonlinear effects on the second-order statistic, which, as we have seen, increases the signal above the values predicted by linear calculations. Nonlinear evolution, however, also changes the distribution function of correlated ellipticity or magnification. In particular, the tails of distribution grow and become asymmetric, reflecting the nonlinear growth of perturbations into small and overdense objects. This leads to a distribution of magnification that is skewed toward positive values. Such skewness is of interest for determining cosmological parameters by itself (Bernardeau et al. 1996), but also affects the inference of cosmological parameters from the measurements of two-point statistics. If the distribution of polarization at a given angular scale θ can be assumed to be normally distributed, then the usual results from Gaussian statistics apply. For example, a single measurement of polarization amplitude within a circular aperture has a Rayleigh probability distribution $\chi^2(2)$, which has an exponentially suppressed tail and from which the limits on cosmological parameters can be derived analytically. Several independent measurements can be easily combined, and only a few observations suffice to obtain strong limits on cosmological parameters. If, on the other hand, the distribution is strongly non-Gaussian, so that the tails of distribution are important, then one cannot use these simple arguments to derive the limits, and a larger set of measurements (a "fair sample") is needed to sample sufficiently the tails so that the variance converges to a true value. At the same time, higher order statistics become easier to measure and can provide further tests of cosmological parameters.

For measurements of density perturbations a simple criterion of where the nonlinear effects become important is $\sigma_R \sim 1$, so for scales above $R \sim 10\ h^{-1}$ Mpc the universe is in the linear regime, and Gaussian statistic can be used. For smaller scales nonlinear effects become important, which leads to deviations from a normal distribution even if the initial field was Gaussian. For projected quantities such as shear and magnification the answer is not so simple. The projection integrates over all the scales, so there will always be contribution from very small and thus very nonlinear scales. On the other hand, projection will reduce the deviations from a Gaussian distribution because of the central limit theorem: if we sum over a sufficiently large number of deflectors, then the final distribution will be a Gaussian regardless of the probability distribution of individual deflectors. We thus expect that the nonlinear effects will be more important for small angles and for bright (nearby) background galaxies.

To obtain a more quantitative answer, we calculated the skewness of local convergence $S = \langle\bar{\kappa}^3\rangle/\langle\bar{\kappa}^2\rangle^{3/2}$ using second-order perturbation theory. Skewness for local convergence does not vanish as in the case of ellipticity (Bernardeau et al. 1996). The second moments of $2\bar{\kappa}$ and $\bar{p}$ are the same, and so one may expect the higher order moments of convergence to be indicative of the nonlinear effects on the ellipticity distribution as well. Note that the quantity S differs from the quantity $s_3 = \langle\bar{\kappa}^3\rangle/\langle\bar{\kappa}^2\rangle^2$ used by Bernardeau et al. (1996). The latter is defined so that it is independent of the amplitude of power spectrum in the

second-order perturbation theory, while S is a more useful variable to quantify the deviations from the Gaussianity. As discussed in the Appendix, second-order perturbation theory should be approximately valid in the regime of interest here, between 1′ to 1°. Second-order perturbation theory accurately estimates the skewness over a much wider range of scales than it does the variance. Only on the smallest scales does it underestimate the skewness, but typically not more than a factor of 2, as shown by N-body simulations (Colombi, Bouchet, & Hernquist 1996). Using the expressions derived in the Appendix (see also Bernardeau et al. 1996) we can compute the value of S for any of the models discussed in this paper. Figure 9 presents the distribution of S as a function of θ for three different redshifts in three different models: flat model with $\sigma_8 = 0.6$, and curvature and cosmological constant models, both with $\sigma_8 = 1$ and $\Omega = 0.3$ (this is very close to the cluster abundance normalization). In all the models we use $\Gamma = 0.25$.

For simplicity we will choose $S = 0.2$ as the value at which the distribution becomes non-Gaussian. For background galaxies at $z_s = 0.5$ we find that the distribution is non-Gaussian even at 4° in the flat model, where the polarization signal is only 0.25%. At $z_s = 1$ and $z_s = 2$ the corresponding values are 1° and 0°.5. For curvature and cosmological constant–dominated models the non-Gaussian effects are even more important because of higher normalization at $8h^{-1}$ Mpc, although the effect is offset by the longer radial distance to a given redshift. The conclusion is that in most of the observationally interesting regime the non-Gaussian effects will be quite important. While this complicates the issue of how large a fair sample should be, it also implies that skewness will be fairly easy to measure with a reasonably small sample. Because s_3 depends sensitively on Ω_m but not on the amplitude of the power spectrum (Bernardeau et al. 1996), this test may become a promising way to determine Ω_m.

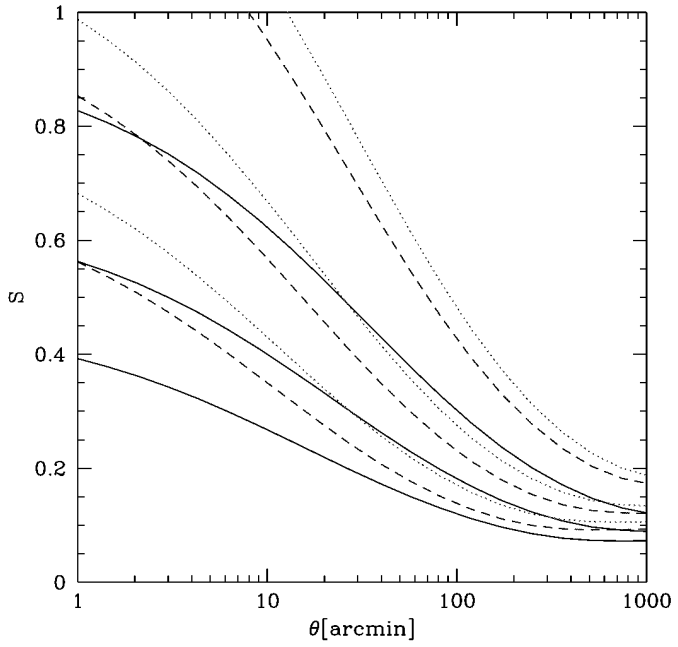

FIG. 9.—Skewness $S = \langle\bar{\kappa}^3\rangle/\langle\bar{\kappa}^2\rangle^{3/2}$ as a function of θ for the flat model (*solid lines*), open model (*dashed lines*), and cosmological constant model (*dotted lines*). The top set of curves is for $z_s = 0.5$, the middle set is for $z_s = 1$, and the bottom set is for $z_s = 2$. Over most of the regime of interest the nonlinear effects are important. Note that for $\theta \lesssim 15'$, the perturbation theory underestimates the skewness of the density (Colombi et al. 1996), so that on arcminute scales S could be nearly a factor of 2 larger than shown in this figure.

The analytical approach presented above provides only a limited view of the properties of ellipticity distribution. For example, such an analysis cannot answer whether skewness is produced by a few outlying points generated by rare clusters, in which case a rather large sample would be needed to sample these properly. A quantitative estimate of what constitutes a fair sample for measuring the variance therefore requires knowledge of at least the fourth moment. Such estimates of a fair sample for measuring the second and third moment can be made more directly by examining the distribution of correlated ellipticities in N-body simulations (Wambsganss, Cen, & Ostriker 1997).

5. DISCUSSION AND CONCLUSIONS

Weak gravitational lensing has several advantages over other probes of LSS. It is directly sensitive to the underlying mass distribution and is therefore independent of biasing, which has plagued many of the cosmological tests based on the distribution of galaxies. While peculiar velocities, in principle, similarly probe the dark matter distribution directly, in practice they suffer because of large observational errors and various biases associated with these. This is the main reason why higher order statistics of velocity fields have not provided strong constraints on cosmological models.

Gravitational lensing could provide a much cleaner way of performing power spectrum and higher order statistical tests, provided that one can overcome observational difficulties and reach the 1% level of polarization, quite feasible with the new generation of composite CCD cameras. For a filled survey with an area θ_0^2 and N measured galaxies, the noise variance in $\bar{p}^2(\theta)$ is given by $\sim(0.4)^2\theta_0/N\theta$, where 0.4 is the typical intrinsic shear for a single galaxy. Although one has to average over a sufficient number of galaxies to reach this level of signal, this is not a severe limitation for sufficiently deep exposures with several hundred thousand galaxies per square degree, so on degree scales the signal-to-noise ratio is of the order of 100 (Kaiser 1997; Fig. 10) and in fact sampling variance (finite number of independent areas of size θ^2) is more important than noise on large angles. On smaller scales the noise increases (proportional to θ^{-1}), but the signal also increases nearly as rapidly, so that the overall signal-to-noise ratio remains approximately flat down to 2′ scales in open and cosmological constant models and slowly decreases in flat models (Fig. 10). Based on this it appears there should be sufficient power present in a survey of this size to measure the signal even on arcminute scales with a high statistical accuracy, so a comparison between small and large scales to constrain Ω_m would indeed be feasible, provided that the systematic effects can be kept under control.

The other limitation at present is that the redshift distribution of background galaxies is unknown beyond $I = 23$ (Lilly et al. 1996; Cowie et al. 1996). New observations with Keck will be able to extend this spectroscopically up to $I = 25$ (e.g., Lowenthal et al. 1997) and even beyond, if spectra of magnified arcs are measured. In addition, weak lensing on high-redshift clusters can be used to constrain the redshift distribution of faint galaxies without measuring their redshifts, although at present there appears to be some controversy over whether the faintest galaxies

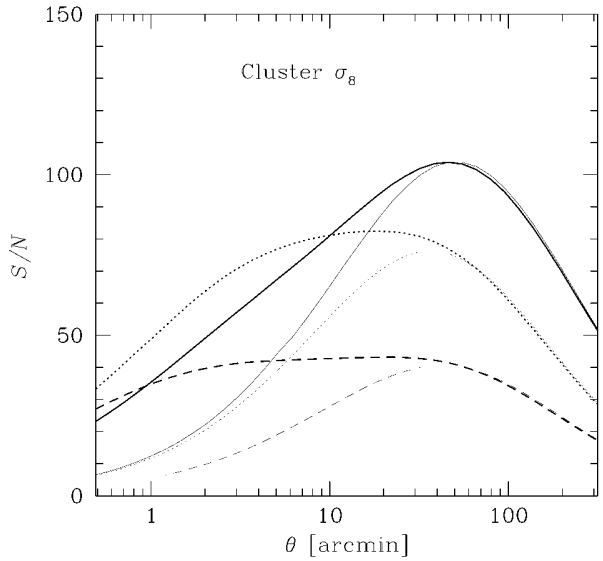

FIG. 10.—The quantity $(\theta/5')\bar{p}^2(\theta)10^5$ is shown for the three models of Fig. 5. This provides an estimate of the signal-to-noise ratio in the measurement of $\bar{p}^2$ in a 1 square degree field with 2×10^5 galaxies, as obtained from a typical observation with a limiting magnitude $I = 26$. Nonlinear evolution causes the curves to be much less sensitive to θ in the range $2' < \theta < 2°$ compared to the linear prediction, which shows a significant peak around $\theta = 1°$. The linear curves for the three models are shown by the thin lines.

are predominantly around or below $z = 1$ (Kneib et al. 1996) or above that (Luppino & Kaiser 1997). Finally, the best hope to constrain their redshift distribution may lie in the photometric redshifts technique (Connolly et al. 1995; Sawicki, Lin, & Yee 1997). This would allow one to perform such precision tests as the growth of power spectrum with redshift, needed to estimate the value of Ω_Λ. For example, based on Hubble Deep Field (HDF) observations, Sawicki et al. (1997) find that the redshift distribution of $I < 27$ galaxies has a large contribution of (predominantly blue) galaxies between redshifts 2–3, while at $I < 25.5$ most of the galaxies are below $z = 1$. In both cases the weak lensing signal-to-noise ratio with these limiting magnitudes would be comparable to the one in Figure 10; thus, in principle, by comparing the signals in the two magnitude bins, it would be straightforward to deduce the value of Ω_Λ. The caveat is that the faintest galaxies in HDF appear to be very irregular and small, so it is not clear whether weak lensing analysis from the ground could be performed on these objects. While more investigation is needed along these lines, there appears to be a real promise of measuring cosmological parameters with future weak lensing observations.

We have analyzed theoretical predictions for weak lensing ellipticity correlations over a broad range of angles and for a variety of cosmological models. Our principal conclusions are the following:

1. The amplitude of the rms ellipticity varies between 4%-6% on arcminute scales to 0.5%–1% on degree scales for background galaxies at $z_s = 1$ and grows as $z_s^{0.6-0.8}$. In this range the amplitude only weakly depends on the value of cosmological parameters if cluster abundance (or velocity flows) normalization is adopted. A single measurement of weak lensing amplitude on $\theta \simeq 15'$ will provide a determination of $\sigma_8 \Omega_m^{0.7-0.8}$, which can be compared with the cluster abundance or velocity flow predictions. Because these tracers all scale similarly with Ω_m, this will not provide an independent determination of Ω_m, for which a more complicated analysis will be needed.

2. Nonlinear effects are important for second-order statistics on scales below 10′ and enhance the signal expected from linear theory. This enhancement can be up to a factor of 2 on arcminute scales. From this it follows that the signal-to-noise ratio does not decrease as rapidly on small scales as expected from linear theory and is, in fact, approximately flat in certain models from arcminute to degree scales (see Fig. 10). Therefore, measurements over this whole angular range should be pursued, especially since they provide complementary information. The interpretation of cosmological models is more cleanly addressed on large angular scales, where nonlinear effects are negligible, and the distribution function is primordial. Small angular scales can provide insight on the nonlinear evolution of perturbations. If our current understanding of the latter is correct, then combining measurements on large and small angular scales will help break the degeneracy between the cosmological parameters, because of different scalings in the linear and nonlinear regimes. The ellipticity on small angles measures $\sigma_8 \Omega_m^{0.5}$, and on large angles it measures $\sigma_8 \Omega_m^{0.8}$, while the variation with z_s can constrain Ω_Λ. Thus, to obtain model-independent measurements of the cosmological parameters, it is necessary to measure the signal over a range of angles and source redshifts.

3. Nonlinear effects on the distribution of ellipticity are significant on scales below 1° and imply that Gaussian statistics cannot be applied to the data. This means that a larger sample will be required to measure second-order statistics than expected from a Gaussian distribution. Conversely, skewness and other higher moments will be easy to measure and may provide a strong test of cosmological parameters independent of the tests above.

In conclusion, weak lensing has the promise to become the next testing ground for cosmological theories. The expected signal-to-noise ratio is above unity over a large range of angles and limiting magnitudes. This should allow one to test sensitively the spectrum of density perturbations and its evolution in time, in both the linear and the nonlinear regimes.

B. J. is very grateful to Jens Villumsen for initiating his interest in weak lensing, and to him and Richhild Moessner for useful discussions. We thank Bernard Fort, Nick Kaiser, Chris Kochanek, Yannick Mellier, Stella Seitz, Simon White, and especially Peter Schneider for stimulating discussions. We thank the referee for suggestions that helped improve the paper and led to the addition of Figure 8.

APPENDIX

In this Appendix we present a general description of lensing in a weakly perturbed universe. The derivation presented here follows Seljak (1995, 1996) and differs from recent derivations in Bernardeau et al. (1996) and Kaiser (1997) in that it employs a

global description of photon trajectories. The geometrical interpretation requires only knowledge of spherical trigonometry, and it is thus particularly simple to derive the general weak lensing expressions. Moreover, it can easily be generalized beyond weak lensing approximation or small deflection angles.

The framework is perturbed Robertson-Walker with small-amplitude metric fluctuations. We will only consider scalar perturbations here, in which case the metric in the longitudinal gauge can be written using conformal time τ and comoving coordinates x^i as follows:

$$ds^2 = a^2(\tau)[-(1 + 2\phi)d\tau^2 + (1 - 2\phi)\gamma_{ij}\,dx^i\,dx^j] \,. \tag{A1}$$

Here $a(\tau)$ is the scale factor expressed in terms of conformal time. We will adopt units such that $c = 1$. We set the two scalar potentials to be equal, which is a good approximation in the matter-dominated epoch. The space part of the background metric can be written as follows:

$$\gamma_{ij}\,dx^i\,dx^j = d\chi^2 + r^2(d\theta^2 + \sin^2\theta\,d\phi^2) \,, \qquad r(\chi) = \sin_K \chi \equiv \begin{cases} K^{-1/2}\sin K^{1/2}\chi \,, & K > 0 \,, \\ \chi \,, & K = 0 \,, \\ (-K)^{-1/2}\sinh(-K)^{1/2}\chi \,, & K < 0 \,, \end{cases} \tag{A2}$$

where K is the curvature term, which can be expressed using the present density parameter Ω (only the present-day density parameter will be used in this paper; hence, we may drop the subscript 0) and the present Hubble parameter H_0 as $K = (\Omega - 1)H_0^2 = -\Omega_K H_0^2$. The relation between the radial distance χ and the redshift z can be obtained from the Friedmann equation, $da/d\chi = H_0(\Omega_m a + \Omega_\Lambda a^4 + \Omega_K a^2)^{1/2}$, where $a = (1 + z)^{-1}$ is the expansion factor, and the densities of matter, cosmological constant and curvature are expressed in terms of the critical density. The density parameter Ω can have contributions from mass density Ω_m or vacuum energy density Ω_Λ, $\Omega = \Omega_m + \Omega_\Lambda$. The advantage of using the conformal time τ is that the metric becomes conformally Euclidean ($K = 0$), three-sphere ($K > 0$), or three-hyperboloid ($K < 0$) and leads to a simple geometrical description of light propagation.

In an unperturbed universe a photon emitted from a source toward the observer will travel along a null geodesic in the radial direction with a radial position given by $\chi = \tau_0 - \tau$. Adding a perturbation changes the photon trajectory. The change in photon direction is governed by the space part of the geodesic equation, which applied to the metric (eq. [A1]) gives

$$\frac{d\boldsymbol{n}}{dl} = 2\boldsymbol{n} \times (\boldsymbol{n} \times \nabla\phi) \equiv -2\nabla_\perp \phi \,, \tag{A3}$$

where the symbol $\nabla_\perp \phi$ denotes the transverse derivative of potential. Null geodesics obey $ds^2 = 0$, from which follows the relation $d\chi = (1 - 2\phi)dl$. Here ϕ can be interpreted as the Newtonian potential, since on scales smaller than the horizon it obeys the cosmological Poisson equation. It can be viewed as providing a force deflecting the photons and affecting their travel time while they propagate through the unperturbed spacetime. Equation (A3) is a generalization of Einstein's deflection angle formula and includes the well-known factor of 2 difference compared to Newtonian gravity. Even when metric perturbations are present, one can continue to parameterize the geodesic with the unperturbed comoving radial distance χ. The deflection angle at a given position χ can be calculated using a locally flat coordinate system, which allows a plane wave expansion for the potential ϕ, provided that the longest correlation length is small compared to the curvature length (this condition is well satisfied for the power spectrum in our universe). The effect of the deflection angle on the photon transverse position must, however, include the curvature effects. In practice, this means that one only needs to know how to solve triangles using the spherical, Euclidean, or hyperboloid trigonometry (Fig. 11). Because the only observable photon direction is that at the observer's position we will propagate photons relative to their final direction (i.e., backward in time). We will also adopt a small deflection angle approximation, because one does not expect large deflection angles due to the lensing, but the expressions can be generalized to remove this restriction. In this approximation the transverse derivatives in equation (A3) can be approximated with the transverse derivatives with respect to the observed direction of the photon or with respect to any other fiducial direction that has a small angular separation with the photon (for example, the unperturbed direction to the source). In this plane approximation the observed photon direction $\boldsymbol{n}$ can be described with a two-dimensional angle $\boldsymbol{\theta}$ with respect to the fiducial direction, $\boldsymbol{n} = (\theta_1, \theta_2, 1 - |\boldsymbol{\theta}|^2/2 \approx 1)$.

Suppose a photon is observed at an angle $\boldsymbol{\theta}$ relative to some fiducial position. As it propagates through the universe, the photon is additionally deflected according to equation (A3) (see Fig. 11). This leads to the transverse photon excursion $\boldsymbol{x}_\perp(\chi)$ relative to the unperturbed line. From Euclidean, spherical, or hyperboloid trigonometry one finds that an individual deflection by $\delta\boldsymbol{\alpha}$ at χ' leads to an excursion at χ given by $\delta\boldsymbol{x}_\perp = \delta\boldsymbol{\alpha}r(\chi - \chi')$. The total excursion is given by an integral over

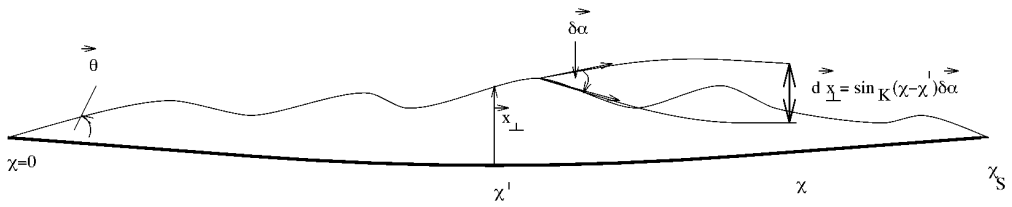

FIG. 11.—Photon propagation relative to the source-observer line: a photon is emitted at the source and observed at the observer's position in the direction $\boldsymbol{\theta}$ relative to the unperturbed source-observer direction (which is curved on an Euclidean plane because of background curvature). A deflection at χ' by $\delta\boldsymbol{\alpha} = -2\nabla_\perp \phi\,\delta\chi$ leads to the transverse excursion at χ given by $\delta\boldsymbol{x}_\perp(\chi) = r(\chi - \chi')\delta\boldsymbol{\alpha}$.

individual deflections,

$$\boldsymbol{x}_\perp(\chi) = -2\int_0^\chi \nabla_\perp \phi(\chi') r(\chi - \chi') d\chi' + \boldsymbol{\theta} r(\chi) \,. \tag{A4}$$

Because of gravitational lensing the "true" surface brightness (i.e., the surface brightness one would see in the absence of any lensing) at position χ_S is mapped into the observed one, $I_{\rm obs}(\boldsymbol{\theta}) = I_{\rm true}(\boldsymbol{\theta} + \delta\boldsymbol{\theta})$, where $\delta\boldsymbol{\theta}$ is the angular deflection of a photon caused by intervening mass, which follows from equation (A4):

$$\delta\boldsymbol{\theta} = \frac{-2}{r(\chi_S)} \int_0^{\chi_S} r(\chi_S - \chi) \nabla_\perp \phi(\chi) d\chi \,. \tag{A5}$$

While the deflection $\delta\boldsymbol{\theta}$ is not directly observable, its gradient is, through the stretching and magnification of distant galaxies. This is described by the two-dimensional shear tensor defined in equation (1). To compute it we expand the potential in equation (A5) across two neighboring rays separated at the observer by $d\theta$ using the *unperturbed* separation $dx = r(\chi) d\theta$. This approximation assumes that the components of shear tensor Φ_{ij} are small (Kaiser 1992), or, similarly, that the relative deflection between the neighboring rays is small compared to the unperturbed separation. This is the so-called weak lensing approximation.

The shear tensor can be diagonalized and decomposed into its trace $2\kappa = \Phi_{11} + \Phi_{22}$ and ellipticity (or polarization) $\boldsymbol{p} = p_1 + ip_2$ given by

$$p_1 = \Phi_{11} - \Phi_{22} \,; \qquad p_2 = 2\Phi_{12} \,. \tag{A6}$$

While trace 2κ magnifies (or demagnifies) the images of galaxies, ellipticity $\boldsymbol{p}$ stretches the images and can be observed by averaging over a sufficient number of galaxies so that the noise caused by the intrinsic ellipticity of galaxies becomes smaller than the signal. The simplest average is the one within a circular window of radius θ, which can be written in Fourier space as

$$\bar{\boldsymbol{p}}(\theta) = \frac{2}{\pi\theta^2} \int_0^\theta d^2\boldsymbol{\theta}' \int_0^{\chi_0} g(\chi) d\chi \int d^3\boldsymbol{k} e^{ik_\chi \chi} e^{i r \boldsymbol{k}_\perp \cdot \boldsymbol{\theta}'} k_\perp^2 \boldsymbol{\beta} \phi(\boldsymbol{k}) \,. \tag{A7}$$

We decomposed the wavevector into the radial component k_χ and the two-dimensional transverse component $\boldsymbol{k}_\perp$ with the amplitude $k_\perp$. We introduced the variables $\beta = \exp(2i\phi_k)$, where ϕ_k is the azimuthal angle of $\boldsymbol{k}_\perp$. The integral over $d^2\boldsymbol{\theta}'$ can be readily performed to give

$$\bar{\boldsymbol{p}}(\theta) = 2\int_0^{\chi_0} g(\chi) d\chi \int d^3\boldsymbol{k} e^{ik_\chi \chi} k_\perp^2 \beta \phi(\boldsymbol{k}) W_2(k_\perp r\theta) \,, \tag{A8}$$

where $W_2(x) = 2J_1(x)/x$. We may now employ the small angle approximation (Limber 1954), which is valid in the limit where the radial window function is broad compared to the typical wavelength that contributes to the integral. In this limit only the modes perpendicular to the radial direction will contribute to the integral, all the others being suppressed because of cancellation of positive and negative fluctuations along the line of sight. This allows one to put $k_\perp \approx k$. With this approximation one obtains for rms ellipticity amplitude $\bar{p}^2 = \bar{\boldsymbol{p}}\bar{\boldsymbol{p}}^*$:

$$\langle \bar{p}^2(\theta) \rangle = 4 \iint d^3\boldsymbol{k}_1 \, d^3\boldsymbol{k}_2 \int_0^{\chi_0} \int_0^{\chi_0} d\chi_1 \, d\chi_2 \, e^{i(k_{\chi 1}\chi_1 + k_{\chi 2}\chi_2)} W_2(k_1 r_1 \theta) W_2(k_2 r_2 \theta) k_1^2 k_2^2 \langle \phi(\boldsymbol{k}_1)\phi(\boldsymbol{k}_2) \rangle \,. \tag{A9}$$

Ensemble average can be expressed in terms of the power spectrum of potential $P_\phi(k)$ or density $P_\delta(k)$,

$$\langle \phi(\boldsymbol{k}_1)\phi(\boldsymbol{k}_2) \rangle = P_\phi(k_1, a) \delta_{\rm D}(\boldsymbol{k}_1 + \boldsymbol{k}_2) = \frac{9}{4} \left(\frac{\Omega_m}{a}\right)^2 \left(\frac{H_0}{k}\right)^4 P_\delta(k_1, a) \delta_{\rm D}(\boldsymbol{k}_1 + \boldsymbol{k}_2) \,, \tag{A10}$$

where power spectrum $P_\delta(k, a)$ and expansion factor a depend on time. Integrating over the Dirac $\delta_{\rm D}$ function and over the radial component of the wavevector, we finally obtain equation (3), which gives the rms amplitude of polarization. The same expression can also be used for rms amplitude of magnification $2\bar{\kappa}$. The rms amplitude for each of the two ellipticity components is simply $1/(2)^{1/2}$ of the total.

Because skewness of ellipticity vanishes for symmetry reasons we will use skewness of local convergence as an estimate of the non-Gaussian nature of ellipticity distribution. Calculating it proceeds along the same lines as for the variance (Bernardeau 1995). It is defined as an ensemble average of the third moment of the mean magnification:

$$\langle \bar{\kappa}^3(\theta) \rangle = \left\langle \left[\int_0^{\chi_0} d\chi \int d^3\boldsymbol{k} e^{ik_\chi \chi} g(\chi) W_2(k_\perp r\theta) k^2 \phi(\boldsymbol{k}) \right]^3 \right\rangle \,. \tag{A11}$$

In linear theory the three-point correlation function vanishes, so one needs to go beyond the linear approximation to obtain a nonvanishing value. In second-order perturbation theory the density field is given by

$$\delta^{(2)}(\boldsymbol{k}) = \int d^3\boldsymbol{k}_1 \, d^3\boldsymbol{k}_2 \, \delta^{(1)}(k_1) \delta^{(1)}(k_2) \delta_{\rm D}(\boldsymbol{k}_1 + \boldsymbol{k}_2 - \boldsymbol{k}) F(\boldsymbol{k}_1, \boldsymbol{k}_2) \,,$$

$$F(\boldsymbol{k}_1, \boldsymbol{k}_2) = \left[\frac{5}{7} + \frac{\boldsymbol{k}_1 \cdot \boldsymbol{k}_2}{k_1^2} + \frac{2}{7} \frac{(\boldsymbol{k}_1 \cdot \boldsymbol{k}_2)^2}{k_1^2 k_2^2} \right] . \tag{A12}$$

Note that the time dependence is all in the growth factors of $\delta(k)$, which is calculated using linear theory (neglecting the extremely weak dependence of $F(\boldsymbol{k}_1, \boldsymbol{k}_2)$ on Ω; see Bouchet et al. 1992). Ensemble averaging of skewness gives six identical terms, which after integrating over the radial wavevectors leads to the following expression:

$$\langle \bar{\kappa}^3(\theta) \rangle = 81\pi^2\theta^{-4}H_0^6 \int_0^{\chi_0} g^3 D^4 \Omega^3 a^{-3} r^{-4}\, d\chi \int d^2\boldsymbol{l}_2\, d^2\boldsymbol{l}_2\, W_2(l_1) W_2(l_2) W_2(|\boldsymbol{l}_1 + \boldsymbol{l}_2|) P_\delta(l_1/r\theta) P_\delta(l_2/r\theta) F(\boldsymbol{l}_1, \boldsymbol{l}_2)\,. \quad \text{(A13)}$$

The integrals can be further simplified using similar manipulations as in Bernardeau (1995), which leads to the following expression:

$$\langle \bar{\kappa}^3(\theta) \rangle = 322\pi^4\theta^{-4}H_0^6 \int_0^{\chi_0} g^3 D^4 \left(\frac{\Omega}{a}\right)^3 r^{-4}\, d\chi \int P\left(\frac{l}{r\theta}\right) W_2^2(l) l\, dl \left[\frac{6}{7}\int P\left(\frac{l}{r\theta}\right) W_2^2(l) l\, dl + \frac{1}{2}\int P\left(\frac{l}{r\theta}\right) W_2(l) W_2'(l) l^2\, dl\right] \quad \text{(A14)}$$

(see also Bernardeau et al. 1996). This expression was used in § 4 to evaluate the importance of nonlinear evolution on the distribution function of polarization.

Several approximations have been employed in obtaining the result above, which limit its validity. Second-order perturbation theory results are only valid in the domain where density perturbations are not much larger than unity, so on very small scales a more involved calculation would be needed. However, these corrections are typically not more than a factor of 2. Because our purpose is to estimate at which scale the non-Gaussian effects become important, second-order perturbation theory suffices. Another approximation is the use of small angle approximation, which leads to corrections on angular scales above 1° (Bernardeau 1995). In the regime of main interest for us, which is between 1′–1°, this is not an important correction. Finally, equation (A14) neglects the deviation of the photon trajectory from the unperturbed path, which also contributes at the second order. This correction is less important than the main term used in equation (A14) and can be neglected (Bernardeau et al. 1996).

REFERENCES

Bardeen, J. M., Bond, J. R., Kaiser, N., & Szalay, A. S. 1986, ApJ, 304, 15
Bernardeau, F. 1995, A&A, 301, 309
Bernardeau, F., van Waerbeke, L., & Mellier, Y. 1996, A&A, submitted
Blandford, R. D., Saust, A. B., Brainerd, T. G., & Villumsen, J. V. 1991, MNRAS, 251, 600
Bouchet, F. R., Juszkiewicz, R., Colombi, S., & Pellat, R. 1992, ApJ, 394, L5
Bunn, E. F., & White, M. 1997, ApJ, 480, 6
Colombi, S., Bouchet, F. R., & Hernquist L. 1996, ApJ, 465, 14
Connolly, A. J., Scabai, I., Szalay, A. S., Koo, D. C., Kron, R. C., & Munn, J. A. 1995, AJ, 110, 2655
Cowie, L. L., Songaila, A., Hu, E. M., & Cohen, J. G. 1996, AJ, 112, 839
Davis, M., Nusser, A., & Willick, J. A. 1996, ApJ, 473, 22
Eke, V. R., Cole, S., & Frenk, C. S. 1996, MNRAS, submitted
Gunn, J. E. 1967, ApJ, 147, 61
Hamilton, A. J. S., Kumar, P., Lu, E., & Matthews, A. 1991, ApJ, 374, L1
Jain, B., Mo, H. J., & White, S. D. M. 1995, MNRAS, 276, L25
Kaiser, N. 1992, ApJ, 388, 272
———. 1997, ApJ, submitted
Keeton, C. R., Kochanek, C. S., & Seljak, U. 1997, ApJ, 482, 604
Kneib, J.-P., Ellis, R. S., Smail, I., Couch, W. J., & Sharples, R. M. 1996, ApJ, 471, 643
Kolatt, T., & Dekel, A. 1997, ApJ, 479, 592
Lahav, O., Lilje, P. B., Primack, J. R., & Rees, M. J. 1991, MNRAS, 251, 128
Lilly, S. J., Le Fevre, O., Hammer, F., & Crampton, D. 1996, ApJ, 460, L1
Limber, D. 1954, ApJ, 119, 655
Lowenthal, J. D., et al. 1997, ApJ, 481, 673
Luppino, G., & Kaiser, N. 1997, ApJ, 475, 20
Miralda-Escude, J. 1991, ApJ, 380, 1
Mould, J., Blandford, R., Villumsen, J., Brainerd, T., Smail, I., Small, T., & Kells, W. 1994, MNRAS, 271, 31
Nityananda, R., & Padmanabhan, T. 1994, MNRAS, 271, 976
Padmanabhan, T., Cen, R., Ostriker, J. P., & Summers, F. J. 1996, ApJ, 466, 604
Peacock, J. A. 1996, MNRAS, in press
Peacock, J. A., & Dodds, S. J. 1996, MNRAS, 780, L19
Peebles, P. J. E. 1980, The Large-Scale Structure of the Universe (Princeton: Princeton Univ. Press)
Pen, U. 1997, ApJ, submitted
Press, W. H., & Schechter, P. 1974, ApJ, 187, 425
Sawicki, M. J., Lin, H., & Yee, H. K. C. 1997, AJ, 113, 1
Seljak, U. 1995, Ph.D. thesis, MIT
———. 1996, ApJ, 463, 1
Stebbins, A. 1996, preprint
Viana, P. T. P., & Liddle, A. R. 1996, MNRAS, 231, 323
Villumsen, J. V. 1996, MNRAS, 281, 369
Wambsganss, J., Cen, R., Xu, G., & Ostriker, J. P. 1997, ApJ, 475, L81
Willick, J. A., Strauss, M. A., Dekel, A., & Kolatt, T. 1997, ApJ, submitted
White, S. D. M., Efstathiou, G., & Frenk, C. S. 1993, MNRAS, 262, 1023